Empirical fit to precision inclusive electron-proton cross sections in the resonance region

M. E. Christy*
Hampton University, Hampton, Virginia 23668, USA

P. E. Bosted†
Thomas Jefferson National Accelerator Facility, Newport News, Virginia 23606, USA
(Received 24 March 2008; revised manuscript received 9 September 2009; published 28 May 2010)

An empirical fit is described to measurements of inclusive inelastic electron-proton cross sections in the kinematic range of four-momentum transfer $0 \leqslant Q^2 < 8$ GeV^2 and final-state invariant mass $1.1 < W < 3.1$ GeV. The fit is constrained by the recent high-precision longitudinal and transverse separated cross section measurements from Jefferson Lab Hall C, unseparated Hall C measurements up to $Q^2 \approx 7.5$ GeV^2, and photoproduction data at $Q^2 = 0$. Compared to previous fits, the present fit covers a wider kinematic range, fits both transverse and longitudinal cross sections, and features smooth transitions to the photoproduction data at $Q^2 = 0$ and deep inelastic scattering data at high Q^2 and W.

DOI: 10.1103/PhysRevC.81.055213 PACS number(s): 25.30.Fj, 13.60.Hb, 14.20.Gk

I. INTRODUCTION

Knowledge of the inclusive electron-proton cross section in the nucleon resonance region is important input for many research activities in nuclear and particle physics. Classic examples include calculations of radiative corrections to cross sections and extractions of spin structure functions from asymmetry measurements. In addition, the latter requires knowledge of the separated longitudinal and transverse photoabsorption cross sections. More recently, the electron-proton resonance region cross section has been used in constraining the vector coupling in models [1,2] of low-energy neutrino-nucleon cross sections. This is important since the quality of low-energy neutrino-nucleon cross section models will become one of the largest uncertainties in the extraction of neutrino oscillation parameters from future long-baseline experiments.

Having the best possible fit to the inclusive electron-proton cross section is important for all the endeavors described above. In this paper, we will describe a fit to precision measurements of inclusive electron-proton cross sections in the resonance region for $Q^2 < 7.5$ GeV^2. Among the advantages of this fit over previous resonance region proton fits [3,4] is the constraint on the individual transverse (T) and longitudinal (L) cross sections afforded by the use of the recent high-precision LT-separated cross section measurements [5,6] from Thomas Jefferson National Accelerator Facility (Jefferson Lab) Hall C, a smooth transition to the photoproduction point, and use of threshold-dependent Breit-Wigner forms for all resonances. It needs to be stressed that while the fit form utilized is, in general, physically motivated, the focus of the current work is to provide the best description of the inclusive proton data and not to determine the masses, widths, transition form factors, or branching ratios of the produced resonant states. These are best determined from exclusive meson production data.

*christy@jlab.org
†bosted@jlab.org

II. INCLUSIVE ELECTRON SCATTERING FROM THE PROTON

In terms of the incident electron energy E, the scattered electron energy E', and the scattering angle θ, the absolute value of the exchanged four-momentum squared in electron-proton scattering is given by

$$Q^2 = (-q)^2 = 4EE'\sin^2\frac{\theta}{2}, \tag{1}$$

and the mass of the undetected hadronic system is

$$W^2 = M_p^2 + 2M_p\nu - Q^2, \tag{2}$$

with M_p the proton mass and $\nu = E - E'$. In these expressions, we have neglected the electron mass which is negligible for the kinematics studied.

In the one-photon exchange approximation, the spin-averaged cross section for inclusive electron-proton scattering can be expressed in terms of the photon helicity coupling as

$$\frac{d\sigma}{d\Omega\, dE'} = \Gamma[\sigma_T(W^2, Q^2) + \epsilon\sigma_L(W^2, Q^2)], \tag{3}$$

where σ_T (σ_L) is the cross section for the photoabsorption of purely transverse (longitudinal) polarized photons,

$$\Gamma = \frac{\alpha E'\left(W^2 - M_p^2\right)}{(2\pi)^2 Q^2 M_p E(1-\epsilon)} \tag{4}$$

is the flux of virtual photons, and

$$\epsilon = \left[1 + 2\left(1 + \frac{\nu^2}{Q^2}\right)\tan^2\frac{\theta}{2}\right]^{-1} \tag{5}$$

is the relative flux of longitudinal virtual photons. Since Γ and ϵ are purely kinematic factors, it is convenient to define the reduced cross section as

$$\sigma_r = \frac{1}{\Gamma}\frac{d\sigma}{d\Omega\, dE'} = \sigma_T(W^2, Q^2) + \epsilon\sigma_L(W^2, Q^2). \tag{6}$$

All the hadronic structure information is, therefore, contained in σ_T and σ_L, which are only dependent on W^2 and Q^2.

In light of the current discrepancy between the proton elastic form factors extracted from unpolarized scattering and those extracted from polarization observables [7], it is worth commenting on the assumed validity of the one-photon exchange approximation. While, the most commonly accepted explanation for resolving this discrepancy is the existence of two-photon (2-γ) exchange contributions to the elastic scattering, the available data indicate that the reduced cross section is still quite linear in ϵ over the ranges measured. Indeed, a recent search for nonlinearities in the combined elastic and inelastic data which separated the longitudinal and transverse cross sections [including a significant portion of the resonance region and the deep inelastic scattering (DIS) data which are fit here] found no significant (i.e., less than 1% typically) evidence for nonlinearities [8]. Hence, although it is impossible to rule out the existence of 2-γ contributions to the inelastic cross sections from these data, the existence of such contributions does not affect our ability to provide a reliable fit to the *measured* cross section data within the one-photon approximation. It is only the separated structure functions that could be incorrectly interpreted if significant 2-γ contributions exist.

III. DESCRIPTION OF THE FIT

In the past, fits to resonance region cross sections have typically not included data covering a large enough range in ϵ and/or of high enough precision to constrain both σ_T and σ_L. Therefore, such fits have relied on an educated guess for the ratio $R = \sigma_L/\sigma_T$ in order to extract data on σ_T from the measured reduced cross sections, and it was the extracted σ_T that was consequentially fit. This guess has typically been to use a fit to DIS data on R extrapolated into the resonance region. The assumption here is that all the resonant structure cancels in R. However, it is now clear from the recent Jefferson Lab LT data [5] that the resonant structure in σ_L differs significantly from that in σ_T, resulting in W- and Q^2-dependent variations of up to 0.1 in R.

Utilizing the new precision data, the reduced cross section was fit by parametrizing $\sigma_T(W^2, Q^2)$ and $\sigma_L(W^2, Q^2)$ and then minimizing the difference of σ_r constructed from Eq. (6) with respect to the data. The cross section parametrization contained 75 free parameters which were determined from the fit: 7 for the resonance masses, 7 for the resonance widths, 25 to describe the Q^2 dependence of the transverse transition form factors, 18 to describe the Q^2 dependence of the longitudinal transition form factors, 10 to describe the nonresonant contribution to σ_T, 7 to describe the nonresonant contribution to σ_L, and a single damping parameter for the delta resonance. A detailed description of the parametrization is given later in this section.

To avoid local minima and to speed up the convergence, the starting parameters for σ_T and σ_L were determined by first fitting the approximate separated cross sections independently. To accomplish this the following procedure was utilized: first, the R_{1998} [9] fit to DIS data on R was used to extract σ_T and σ_L from σ_r; second, the extracted data on σ_T and σ_L were fit independently; and finally, R determined from the new fits was used to extract σ_T and σ_L for the next iteration. Several iterations were performed to ensure that reasonable convergence was obtained. The fit forms for the resonant and nonresonant contributions to the cross sections were determined from this procedure for both σ_T and σ_L and were then used in a single fit to σ_r in which all transverse and longitudinal parameters were allowed to vary simultaneously.

The fit form used to describe the separated resonance region photoabsorption cross sections was based on the following ansatz: (1) the cross section is the incoherent sum of contributions from resonance production (σ^R) and a nonresonant background (σ^{NR}), (2) the resonant cross section can be described by threshold-dependent relativistic Breit-Wigner forms with Q^2-dependent amplitudes for each resonance, and (3) the nonresonant background varies smoothly with W^2. Therefore,

$$\sigma_{T,L}(W^2, Q^2) = \sigma^R_{T,L} + \sigma^{\mathrm{NR}}_{T,L}, \tag{7}$$

with resonant contribution

$$\sigma^R_{T,L}(W^2, Q^2) = W \sum_{i=1}^{7} \mathrm{BW}^i_{T,L}(W^2)\left[A^i_{T,L}(Q^2)\right]^2. \tag{8}$$

The Breit-Wigner form utilized is

$$\mathrm{BW}^i = \frac{K_i K_i^{\mathrm{c.m.}}}{K K^{\mathrm{c.m.}}} \frac{\Gamma_i^{\mathrm{tot}} \Gamma_i^{\gamma}}{\Gamma_i\left[\left(W^2 - M_i^2\right)^2 + \left(M_i \Gamma_i^{\mathrm{tot}}\right)^2\right]}, \tag{9}$$

with

$$K = \frac{W^2 - M_p^2}{2M_p}, \tag{10}$$

$$K^{\mathrm{c.m.}} = \frac{W^2 - M_p^2}{2W}, \tag{11}$$

$$K_i = K|_{M_i}, \tag{12}$$

and

$$K_i^{\mathrm{c.m.}} = K^{\mathrm{c.m.}}|_{M_i}. \tag{13}$$

Here, K and $K^{\mathrm{c.m.}}$ represent the equivalent photon energies in the laboratory and center of mass (c.m.) frames, respectively, while K_i and $K_i^{\mathrm{c.m.}}$ represent the same quantities evaluated at the mass of the ith resonance, M_i. Γ_i^{tot} is the full decay width defined by

$$\Gamma_i^{\mathrm{tot}} = \sum_{j=1}^{3} \beta_i^j \Gamma_i^j, \tag{14}$$

with β_j^i the branching fraction to the jth decay mode for the ith resonance, and Γ_i^j the partial width for this decay mode. For single-meson decay modes, the partial widths were determined from

$$\Gamma_i^j = \Gamma_i \left[\frac{p_j^{\mathrm{c.m.}}}{p_j^{\mathrm{c.m.}}|_{M_i}}\right]^{2l+1} \left[\frac{\left(p_j^{\mathrm{c.m.}}|_{M_i}\right)^2 + X_i^2}{\left(p_j^{\mathrm{c.m.}}\right)^2 + X_i^2}\right]^l, \tag{15}$$

where Γ_i are the intrinsic widths of each resonance, the $p_j^{\mathrm{c.m.}}$ are meson momenta in the center of mass, l is the angular momentum of the resonance, and X_i is a damping parameter. In the present analysis, it was found that a good fit to the data was obtained using $X_i = 0.215$ GeV for all the resonances except the $P_{33}(1232)$, where a smaller value of

$X_1 = 0.1446$ GeV resulted in a modest improvement. Overall the goodness of the fit was found to be relatively insensitive to the exact value of X_i. For the two-pion decay mode, the partial widths were determined from

$$\Gamma_i^j = \frac{W\Gamma_i}{M_i}\left[\frac{p_j^{\text{c.m.}}}{p_j^{\text{c.m.}}|_{M_i}}\right]^{2l+4}\left[\frac{\left(p_j^{\text{c.m.}}|_{M_i}\right)^2 + X_i^2}{\left(p_j^{\text{c.m.}}\right)^2 + X_i^2}\right]^{l+2}. \quad (16)$$

The virtual-photon width was defined by

$$\Gamma_i^\gamma = \Gamma_i\left[\frac{K^{\text{c.m.}}}{K^{\text{c.m.}}|_{M_i}}\right]^2\left[\frac{(K^{\text{c.m.}}|_{M_i})^2 + X_i^2}{(K^{\text{c.m.}})^2 + X_i^2}\right]. \quad (17)$$

A. Constraints on the Q^2 dependence for σ_L

There were several physics constraints on the Q^2 dependence of the cross section which were realized in the fit form. For instance, the longitudinal cross section must vanish at the photoproduction point due to current conservation and at large Q^2 due to helicity conservation in scattering from spin-1/2 fermions. These constraints were independently imposed in both the resonant and nonresonant contributions to the cross section. This was accomplished for the resonant contribution by a suitable form for the longitudinal transition amplitudes, which vanished at $Q^2 \to 0$ and $Q^2 \to \infty$.

B. Resonances included in the fit

Seven possible resonance contributions were included in the fit to σ_T and represent those with the largest photocouplings to the proton as listed by the Particle Data Group [10]. These consisted of the first prominent resonance, the Δ $P_{33}(1232)$, two states in the second resonance region, the $S_{11}(1535)$ and the $D_{13}(1520)$, and two in the third resonance region, the $S_{15}(1650)$ and the $F_{15}(1680)$. In addition, the Roper, $P_{11}(1440)$, and a broad resonance around $W \approx 1.9$ GeV were included. Only the pion, η, and two-pion decay modes were included for each resonance, and the branching fractions used are given in Table I. The region at $W \approx 1.9$ GeV is occupied by many states and was assigned an angular momentum of $l = 3$ in the fit. We have not tried to be exhaustive by including all known resonant states, but have, rather, tried to include enough of the dominant states to provide for a good fit to the data without requiring a burdensome number of additional parameters. For recent reviews of electromagnetic meson production in the nucleon resonance region, we refer the reader to Ref. [11] and to the latest fit to the unitary isobar model, MAID2007 [12].

TABLE I. Resonance number I, name (and quantum numbers), and branching fractions for the resonant states included in the fit.

I	State	$\beta_{1\pi}$	$\beta_{2\pi}$	β_η
1	$P_{33}(1232)$	1.0	0.0	0.0
2	$S_{11}(1535)$	0.45	0.10	0.45
3	$D_{13}(1520)$	0.65	0.35	0.0
4	$F_{15}(1680)$	0.65	0.35	0.0
5	$S_{15}(1650)$	0.4	0.5	0.1
6	$P_{11}(1440)$	0.65	0.35	0.0
7	($l = 3$ assumed)	0.5	0.5	0.0

The resonances included for σ_L were largely the same as for σ_T. However, due to the decreased sensitivity of the cross section data to σ_L, it was found that including more than a single resonance in the region of the $D_{13}(1520)$ and $S_{11}(1535)$ around $W \approx 1.5$ had little impact on the goodness of the fit. Therefore, the second resonance listed in Table I [$S_{11}(1535)$] was not included in the fit for σ_L. The choice of excluding this particular resonance was arbitrary, because it was found that excluding the $D_{13}(1520)$ instead had a negligible impact.

C. Resonance transition amplitudes

For the transverse resonance transition amplitudes, the fit form utilized was

$$A_T^i(Q^2) = \frac{A_T^i(0)}{(1 + Q^2/0.91)^{c_i}}\left(1 + \frac{a_i Q^2}{1 + b_i Q^2}\right), \quad (18)$$

while for the longitudinal resonance transition amplitudes the fit form utilized was

$$A_L^i(Q^2) = A_L^i(0)\frac{Q^2}{(1 + d_i Q^2)}e^{-e_i Q^2}. \quad (19)$$

For large Q^2, $A_T^i(Q^2)$ reduces to

$$A_T^i(Q^2) = \frac{A_T^i(0)}{(1 + Q^2/0.91)^{c_i}}\frac{a_i}{b_i}, \quad (20)$$

which is just the dipole form for $c_i = 2$. For $Q^2 \to 0$, $A_T^i(Q^2)$ linearly approaches the photoproduction value, $A_T^i(0)$, while $A_L^i(Q^2)$ linearly vanishes.

D. Nonresonant background

For the nonresonant part of the transverse cross section, the fit form which was found to describe the data well was

$$\sigma_T^{\text{NR}} = x'\sum_{i=1}^{2}\frac{\sigma_T^{\text{NR},i}(0)}{\left(Q^2 + a_i^T\right)^{[b_i^T + c_i^T Q^2 + d_i^T Q^4]}}(\Delta W)^{i+1/2}, \quad (21)$$

where

$$x' = \left(1 + \frac{W^2 - (M_p + m_\pi)^2}{Q^2 + Q_o^2}\right)^{-1}, \quad (22)$$

with m_π the pion mass, $Q_0^2 = 0.05$ GeV^2, and $\Delta W = W - (M_p + m_\pi)$. Previous resonance region fits have also included terms to describe the W dependence with $(\Delta W)^{i+1/2}$. However, these did not attempt to fit beyond $W \approx 2$ GeV, where, in contrast to the data, this particular form continues to rise with increasing W^2. Here it was found that this rise

TABLE II. Summary of data sets included in the fit.

Data set	Q^2_{min} (GeV^2)	Q^2_{max} (GeV^2)	# Data points
E94-110 [5]	0.18	5	1259
E00-116 [14]	3.6	7.5	256
E00-002 [15]	0.06	2.1	1346
SLAC DIS [16]	0.6	9.5	296
Photoproduction (Old) [17–19]	0	0	242
Photoproduction (DAPHNE) [20]	0	0	57

TABLE III. Fit parameters for each resonance I, as defined in the text. Units of cross section are μb and all masses, momenta, and energies are in units of GeV. In addition to these parameters, the delta damping factor X_1 was determined from the fit.

I	M_i	Γ_i	$A_T^i(0)$	a_i	b_i	c_i	$A_L^i(0)$	d_i	e_i
1	1.230	0.136	7.780	4.229	1.260	2.124	29.4140	19.910	0.226
2	1.530	0.220	6.335	6823.200	33521.000	2.569	0.0	–	–
3	1.506	0.083	0.603	21.240	0.056	2.489	157.9200	97.046	0.310
4	1.698	0.096	2.330	−0.288	0.186	0.064	4.2160	0.038	1.218
5	1.665	0.109	1.979	−0.562	0.390	0.549	13.7640	0.314	3.000
6	1.433	0.379	0.0225	462.130	0.192	1.914	5.5124	0.054	1.309
7	1.934	0.380	3.419	0.000	0.000	1.000	11.0000	1.895	0.514

can be moderated by the additional x' factor. This allows a good fit to the data to be obtained up to $W = 3.2$ GeV. The factor $x' \approx x = Q^2/2M_p\nu$ for $W^2 - M_p^2 \gg M_p m_\pi$ and $Q^2 \gg Q_0^2$, but has the important properties required to fit the entire resonance data set, so that it approaches a constant for $Q^2 \to 0$ and vanishes at the pion threshold.

For the longitudinal cross section, it was found that the nonresonant background could *not* be well described by powers of $W^{1/2}$ at fixed Q^2, but was better represented away from the pion threshold by $(1-x)^a$. Therefore, the form utilized was

$$\sigma_L^{\rm NR} = \sum_{i=1}^{1} \sigma_L^{{\rm NR},i}(0) \frac{(1-x')^{[a_i^L t + b_i^L]}}{(1-x)} \times \frac{(Q^2)^{c_i^L}}{\left(Q^2+Q_0^2\right)^{(1+c_i^L)}} (x')^{[d_i^L + e_i^L t]}, \quad (23)$$

where

$$t = \frac{\ln\left(\ln\frac{Q^2+m_0}{0.33^2}\right)}{\ln\frac{m_o}{0.33^2}} \quad (24)$$

is a slowly varying function of Q^2. For $\sigma_L^{\rm NR}$, we used $Q_0^2 = 0.125$ GeV^2 and $m_0 = 4.2802$ GeV.

IV. THE DATA SETS

A summary table of the data sets, including the number of data points and the Q^2 range of each set, is provided in Table II.

The nucleon resonance region ($W < 2$ GeV) electron-proton (ep) scattering data included in the fit came principally from a series of Jefferson Lab Hall C experiments which utilized the well-understood High Momentum Spectrometer (HMS). The various Hall C data sets have been estimated

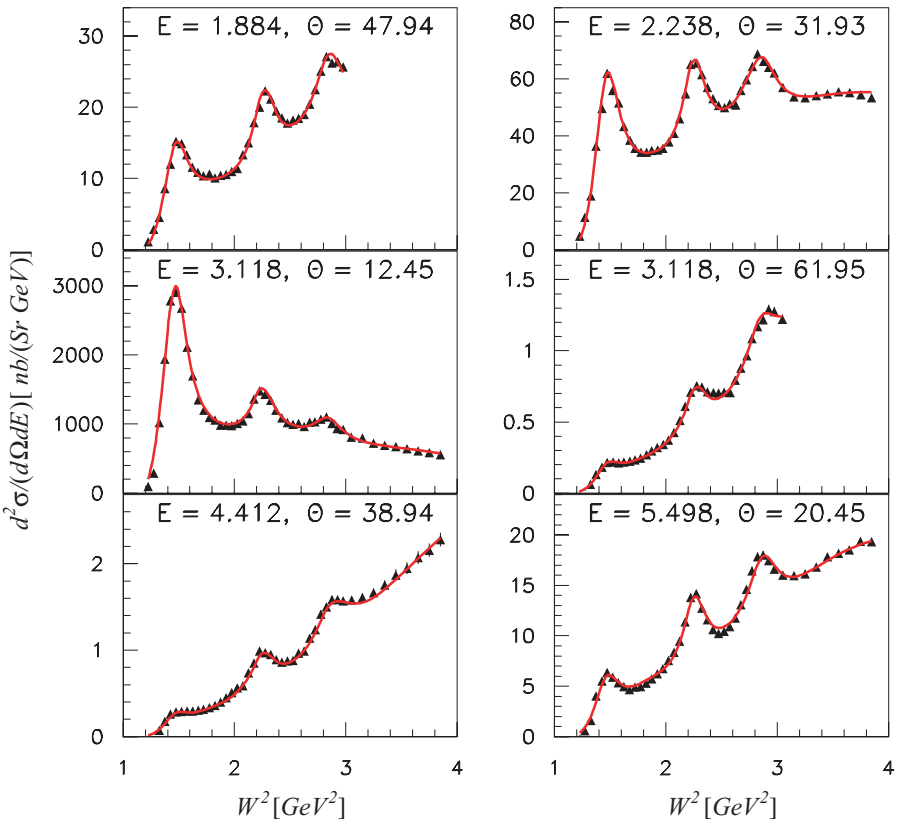

FIG. 1. (Color online) Comparison of the fit results (solid lines) to the JLab E94-110 resonance region data [5,6] (solid triangles) versus W^2, for several representative kinematic settings. Beam energies E are in GeV, and electron scattering angles θ are in degrees.

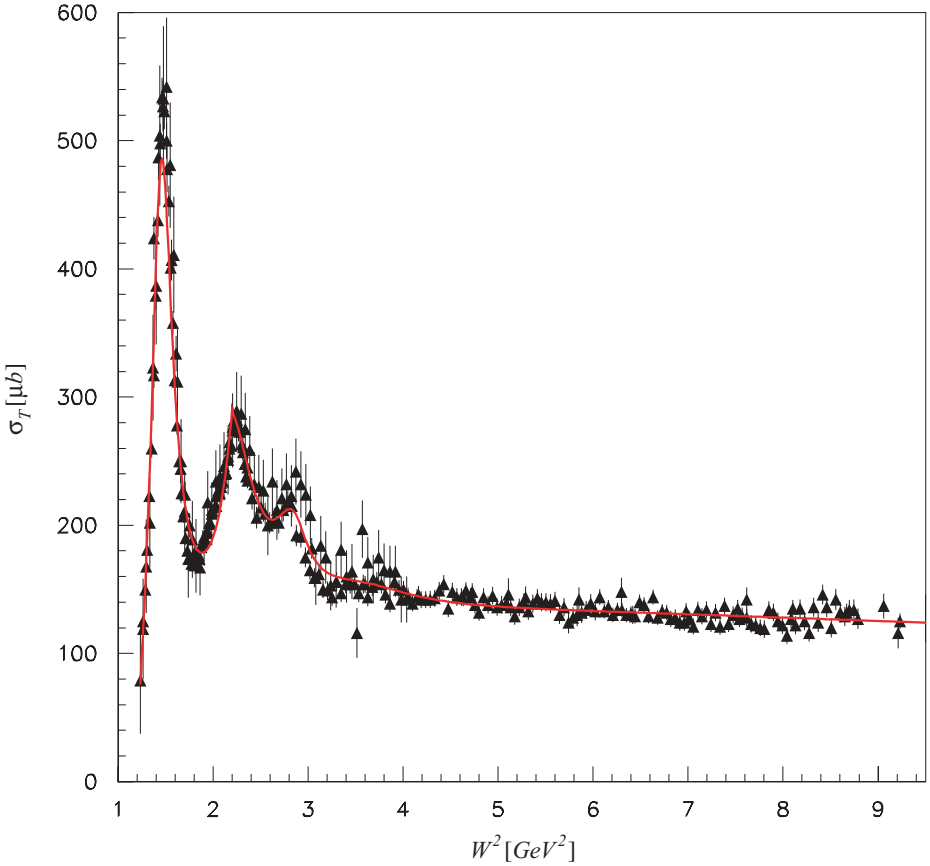

FIG. 2. (Color online) Comparison of fit (solid line) to the photoproduction data used in the fit (see Table II).

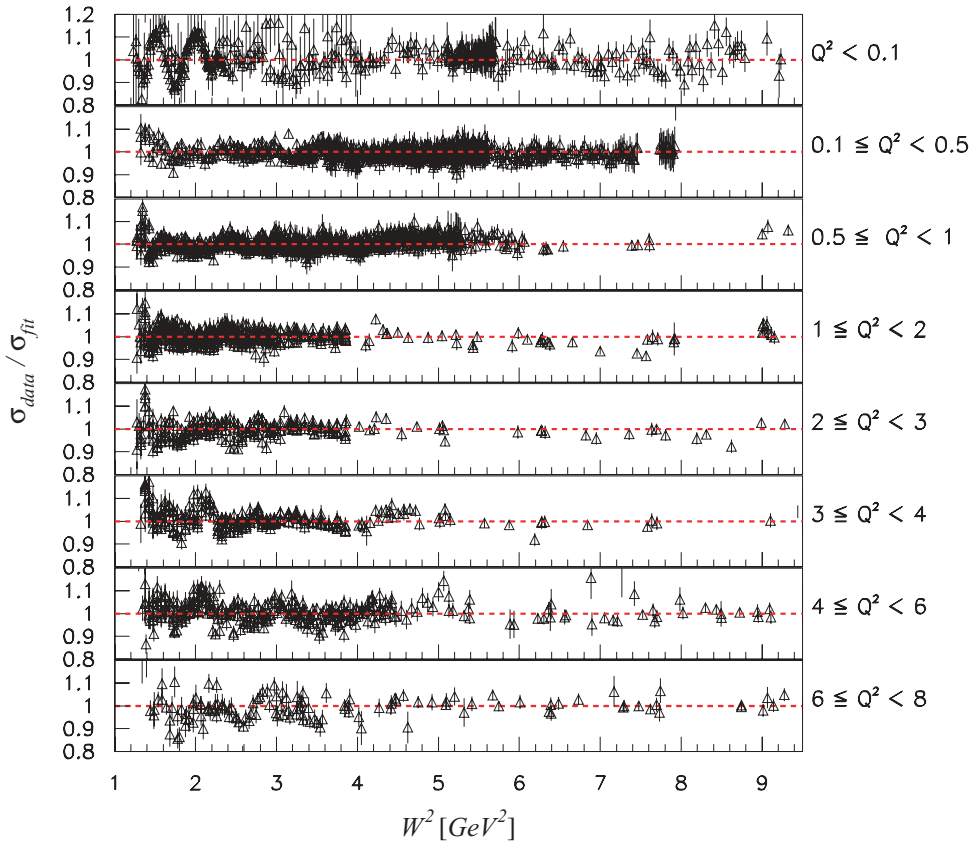

FIG. 3. (Color online) Ratio of all fitted cross section data to the fit results at the eight Q^2 ranges indicated. The units of Q^2 are GeV^2.

to have normalization uncertainties of ≈2% and were found to agree in their regions of kinematic overlap to better than 1%. There also exists a large body of inclusive *ep* data from the Hall B CLAS Collaboration in the kinematic region fit. However, in addition to having significantly larger systematic uncertainties, only results for the F_2 structure function have been published. Therefore, these data were not utilized, since only cross section data were fit.

For $0.18 < Q^2 < 4.5$, the inclusive proton data utilized were dominated by the recent E94-110 high-precision data [5], which have typical point-to-point uncertainties in ϵ of less than 2%. This experiment was optimized to separate σ_L and σ_T from Rosenbluth separations [13] and, therefore, provided a significant ϵ range at fixed W^2 and Q^2 for constraining the separated cross sections. For $4.5 < Q^2 < 7.5$, the resonance data are mainly from the E00-116 experiment [14]. For this data set, the uncertainties were typically statistically dominated. In addition, the cross sections at each W^2 and Q^2 were only measured at a single kinematic setting and, hence, these data did not provide any ϵ range to constrain σ_L and σ_T when taken by themselves. Preliminary data from E00-002 [15] were used to extend the Q^2 range of precision data down to 0.05 GeV^2. Data in the DIS region [16] ($W > 2$) were used to constrain the fit up to $W = 3.1$ GeV. Several sets of photoproduction data were used to constrain the fit at $Q^2 = 0$ GeV^2: data taken prior to 1975 [17–19] and the more recent data from DAPHNE [20]. While the latter is much more precise, it does not extend beyond the second resonance region.

TABLE IV. Values for the transverse (T) and longitudinal (L) nonresonant fit parameters. The units of cross section are μb and all masses, momenta, and energies are in units of GeV. In addition to those listed, the parameters Q_0 and m_o which determine the transition of σ_T^{NR} to $Q^2 = 0$ were determined from the fit.

L,T	i	$\sigma_{L,T}^{\mathrm{NR},i}$ (0)	a_i	b_i	c_i	d_i	e_i
T	1	246.1	0.0675	1.3501	0.1205	−0.0038	–
T	2	−89.4	0.2098	1.5715	0.0907	0.0104	–
L	1	86.7	0.0000	4.0294	3.1285	0.3340	4.9623

V. RESULTS AND DISCUSSION

The results for the fit parameters are given in Tables III and IV. Overall, the fit presented here provides an excellent description of the resonant structures seen in inclusive *ep* cross sections, as illustrated in Fig. 1 for representative kinematic settings of the E94-110 experiment [5]. The fit does a reasonable job in describing the photoproduction data [17–20] (see Fig. 2), although it was not possible to obtain a perfect

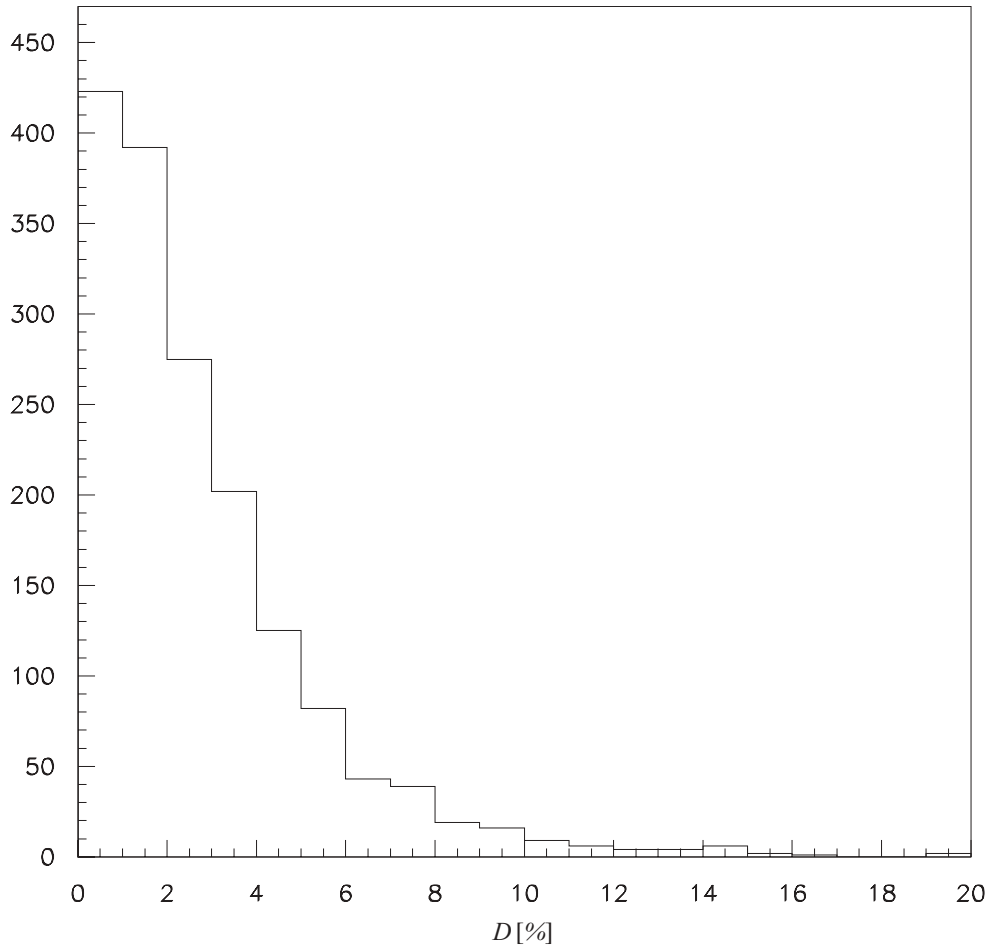

FIG. 4. Frequency distribution for the percent differences of the data to the fit for $Q^2 > 0$.

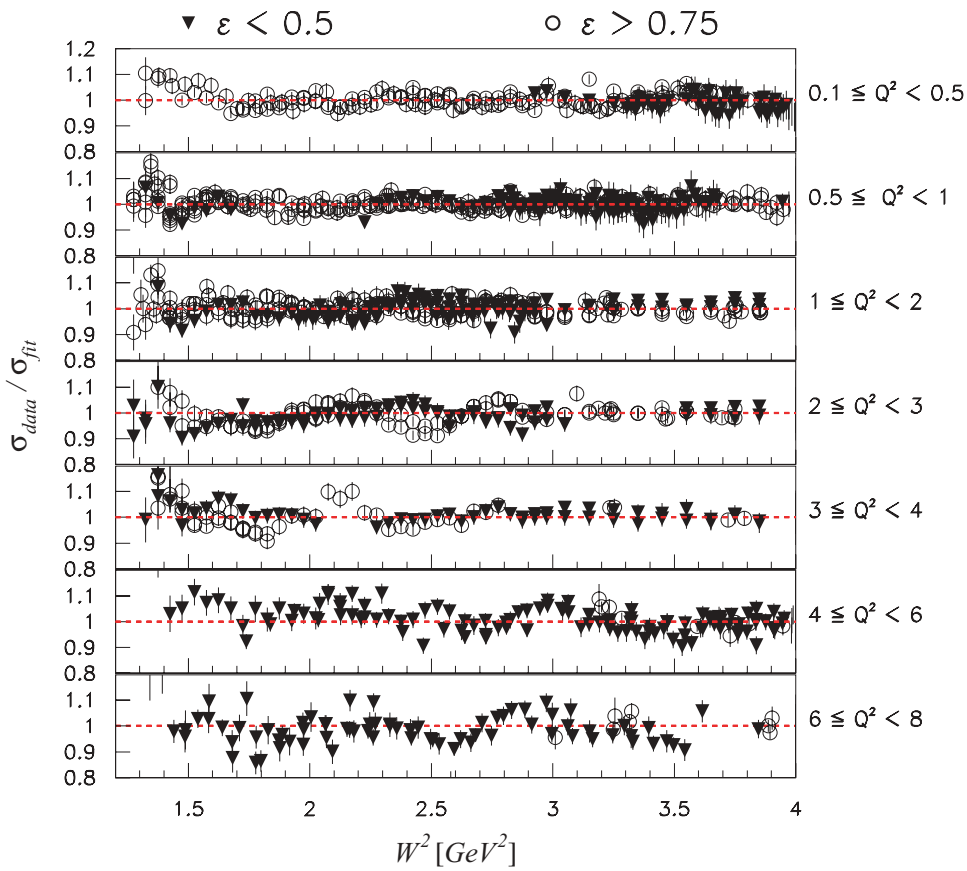

FIG. 5. (Color online) Ratio of selected cross section data to the fit at the seven Q^2 ranges indicated (Q^2 in units of GeV^2). The data for $\epsilon < 0.5$ are shown as the solid triangles, while the data with $\epsilon > 0.75$ are shown as the open circles.

description of the dip region between the $\Delta(1232)$ and the second resonance region. This is illustrated more clearly in Fig. 3, where two significant oscillations around unity are observed at low W and $Q^2 < 0.1$ GeV^2 (dominated by the photoproduction data). This is likely due to the Q^2 dependence for the transverse transition form factors chosen. It is certainly true that the individual transverse transition form factors in the second resonance region are *not* consistent with those extracted from exclusive analysis [11], although there is consistency in the overall transverse resonance strength in this region. Part of this inconsistency could be caused by the chosen form for the Roper amplitude A_T^2. Recent data [11] indicate that this amplitude decreases to zero by $Q^2 \approx 0.4$ GeV^2 and then increases again with increasing Q^2. Such a Q^2 dependence is not possible with our chosen form for A_T^2, and this could force a shifting of strength between the various resonances in this region which is Q^2 dependent. This is a topic that will be pursued in future fitting studies.

The quality of the fit is quite good, overall, with nearly all data points differing from the fit by less than 5%, and more than half of the data points deviating from the fit by less than 3% as evidenced by Fig. 4. As illustrated in Fig. 5, the fit describes data both at low ϵ and high ϵ reasonably well. This is especially true for $Q^2 < 2$ where the available data show little or no variation in the goodness of the fit for differing ϵ values, indicating that both the transverse and longitudinal cross sections are well represented here. The data from E94-110 clearly indicate that the resonance structure in the longitudinal cross section becomes enhanced relative to the background for Q^2 between 2 and 3 GeV, and that the resonance peaks prefer widths that are narrower than for the transverse cross section. This indicates that the description of the data could be improved by allowing the resonance width parameters to be varied independently for the longitudinal cross section.

The largest deviation with ϵ is in the dip region between the second and third resonance region for $2 < Q^2 < 4$ GeV^2. This is mainly due to the difficulty in fitting the W^2 dependence of the longitudinal cross section here. This region is dominated by the E94-110 data [5], which indicate significant resonance structure in the longitudinal channel in this Q^2 range, but with the longitudinal strength dipping very close to zero in the dip region [5]. This is inconsistent with a fit form for the nonresonant cross section which decreases monotonically as the pion threshold is approached, and could indicate that our assumption of incoherency between the resonant and nonresonant scattering is starting to fail. Due to the lack of low ϵ data at high Q^2 and $W < 2$ GeV, the fit for σ_L does rely to some extent on the extrapolation in Q^2 of the fit form used.

VI. CONCLUSIONS

In summary, we have developed a fit to the total inclusive transverse and longitudinal proton cross section that describes existing data at the 3% or better level over almost the entire range $0 \leqslant Q^2 < 8$ GeV^2 and $1.1 < W < 3.1$ GeV, corresponding to the kinematic settings available at Jefferson

Lab with a 6 GeV beam. The fit can therefore be used to reliably evaluate radiative corrections and to extract spin structure functions from asymmetry measurements. The fit also provides a convenient representation of world data that can be used for the experimental evaluation of the high-x contribution to sum rules involving integrals over proton structure functions.

The FORTRAN computer code embodying the fit described in this article is available by email request from the authors. Tables of cross section data fit can be found in the relevant references, except for the preliminary data from JLab E00-002, which will be made available from the Hall C website at www.jlab.org/resdata. This webpage will be utilized as a repository for the final cross sections, as well as all available resonance region cross section data and fits.

ACKNOWLEDGMENTS

We thank V. Tvaskis for compiling the preliminary data table for Ref. [15]. This work was supported in part by research grants 0099540 and 9633750 from the National Science Foundation. The Southeastern Universities Research Association (SURA) operated the Thomas Jefferson National Accelerator Facility for the US Department of Energy under Contract No. DE-AC05-84ER40150.

[1] E. A. Paschos, I. Schienbein, and J.-Y. Yu, arXiv:0704.1991.
[2] O. Lalakulich and E. A. Paschos, Acta Phys. Polon. B **37**, 2311 (2006); Phys. Rev. D **71**, 074003 (2005).
[3] L. M. Stuart *et al.*, Phys. Rev. D **58**, 032003 (1998).
[4] I. Niculescu, Ph.D. thesis, Hampton University, 1999.
[5] Y. Liang *et al.*, arXiv:nucl-ex/0410027 (revised March 3, 2008).
[6] Y. Liang, Ph.D. thesis, American University, 2003.
[7] J. Arrington, W. Melnitchouk, and J. A. Tjon, Phys. Rev. C **76**, 035205 (2007).
[8] V. Tvaskis, J. Arrington, M. E. Christy, R. Ent, C. E. Keppel, Y. Liang, and G. Vittorini, Phys. Rev. C **73**, 025206 (2006).
[9] K. Abe *et al.*, Phys. Lett. B **452**, 194 (1999).
[10] C. Amsler *et al.* (Particle Data Group), Phys. Lett. B **667**, 1 (2008).
[11] V. D. Burkert and T. S. H. Lee, Int. J. Mod. Phys. E **13**, 1035 (2004).
[12] D. Drechsel, S. S. Kamalov, and L. Tiator, Eur. Phys. J. A **34**, 69 (2007).
[13] M. N. Rosenbluth, Phys. Rev. **79**, 615 (1956).
[14] S. P. Malace *et al.* (Jefferson Lab E00-116 Collaboration), Phys. Rev. C **80**, 035207 (2009).
[15] Preliminary results from JLab E00-002 Collaboration, C. Keppel and M. I. Niculescu, spokespersons. Data files can be obtained at [hallcweb.jlab.org/resdata].
[16] L. W. Whitlow, Ph.D. thesis, American University, 1990.
[17] E. D. Bloom *et al.*, SLAC-PUB-0653, 1969 (unpublished).
[18] T. A. Armstrong *et al.*, Phys. Rev. D **5**, 1640 (1972).
[19] H. Meyer *et al.*, Phys. Lett. B **33**, 189 (1970).
[20] M. MacCormick *et al.*, Phys. Rev. C **53**, 41 (1996).